CHEMISTRY & CHEMICAL TECHNOLOGY

Chem. Chem. Technol., 2026,
Vol. 20, No. 1, pp. 183–199

Chemistry

DESIGN AND SYNTHESIS OF IMIDAZOLE-BASED LIGAND AND ITS METAL COMPLEXES: SPECTROSCOPIC CHARACTERIZATION AND EVALUATION OF ANTIBACTERIAL, ANTIOXIDANT AND HEMOLYTIC ACTIVITIES

Howraa A. Khudair[1], Sawsan K. Abbas[2], Suhad K. Abbas[1,✉]

[1] Department of Chemistry, College of Science, University of Kerbala, Karbala, Iraq
[2] Department of Chemistry, College of Education for Pure Science, University of Kerbala, Karbala, Iraq
✉ *suhad.k@uokerbala.edu.iq*

https://doi.org/10.23939/chcht20.01.183

Abstract. In this study, new complexes containing a multi-substituted aryl imidazole ligand, namely (2-(1H-phenanthro[9,10-d] imidazol-2-yl) phenol, have been synthesized. Imidazole ligand L was synthesized *via* a condensation reaction between diketone (9,10-phenathroquinone), aromatic aldehyde (2-hydroxy benzaldehyde), and ammonium acetate in the presence of glacial acetic acid as a solvent and catalyst. Subsequently, metal complexes were prepared by reacting this ligand with transition metal salts, including Fe (II), Cu (II), Ni (II), and Co(II) chlorides, in an appropriate solvent like ethanol under controlled temperature and stirring conditions to ensure the formation of stable complexes. The structures of the ligands and their metal complexes were characterized utilizing different spectroscopic techniques, such as (UV-Vis), FT-IR, ^{1}H NMR, ^{13}C NMR spectroscopic, mass spectroscopy, magnetic susceptibilities, molar conductivity, and elemental analysis (C. H. N). It is observed that the synthesized complexes have tetrahedral and octahedral geometrical structures. The ligand and its complexes play important roles in supramolecular assemblies because they can also provide bidentate N-donor sites for chelating with metal ions to form a bridge ligand. The biological evaluation was performed using the agar well diffusion method to assess the antibacterial activity of both ligand and metal complexes against selected Gram-positive and Gram-negative bacterial strains. The results revealed that the free ligand and its metal complexes displayed significantly enhanced antibacterial activity compared to the reference drug. Antioxidant potential was assessed using the DPPH radical scavenging assay; metal complexes generally showed higher radical inhibition percentage. Hemolytic activity was evaluated on human red blood cells to determine cytocompatibility. The findings showed that the ligand and metal complexes exhibited low to moderate hemolytic activity, indicating acceptable biocompatibility for potential biomedical applications.

Keywords: 9,10-phenathroquinone, imidazole ligand, complexes, antibacterial activity, antioxidant potential.

1. Introduction

Imidazole is a nitrogen-containing heterocyclic compound[1] that forms the structural core of many biologically important molecules.[2] Its five-membered aromatic ring contains two nitrogen atoms in non-adjacent positions,[3] allowing it to participate in numerous chemical and biological processes.[4] Natural imidazole derivatives include histidine and histamine,[5] which play essential roles in enzyme function,[6] neurotransmission,[7] and immune responses. Thanks to its electron-rich nitrogen atoms,[8] the imidazole ring can participate in hydrogen bonding and metal ion coordination, making it an ideal pharmacophoric vehicle for drug design.[9] Imidazole derivatives are known for their broad range of biological activities, including antiviral,[10] antifungal,[11] anti-inflammatory,[12] anticancer, antimicrobial, and antioxidant properties.[13] Many pharmaceuticals contain imidazole rings, such as metronidazole (antimicrobial), ketoconazole (antifungal), and cimetidine (antiulcer). These biological effects stem from the ring's ability to interact with enzymes, DNA, and receptor proteins,[14] thereby affecting vital biochemical pathways.[15] Furthermore, substitutions in the imidazole ring allow for fine-tuning of the electronic and steric properties, enabling selective activity against specific targets.[16] Metal

complexes play a pivotal role in modern drug design,[17] as they significantly impact the physical, chemical,[18] and biological properties of pharmaceutical compounds.[19] Coordinating biologically active ligands with metal ions often improves the compound's stability, solubility, and bioavailability.[20] In addition, metal complexes may have mechanisms of action different from those of the free ligand, enhancing their selectivity and efficacy against specific biological targets.[21] Transition metals, such as copper, nickel, and zinc, are among the most widely used elements in this field due to their unique catalytic and redox properties,[22] which contribute to their antimicrobial, anticancer, and antioxidant properties when coordinated with appropriate organic ligands.[20] Chelating also plays a role in modifying the properties of a drug compound, such as its lipophilicity and membrane permeability,[23] facilitating its absorption and increasing its effectiveness within cells.[24] Often, metal-complex-based drugs exhibit synergistic effects, with both the metal ion and the organic ligand contributing to the overall therapeutic activity. A prominent example of this class is cisplatin, a platinum compound used as an anticancer agent, along with sulfur-containing metal complexes used as antimicrobials.[25] Accordingly, metal complexes represent a promising strategy for developing multi-targeted therapeutic agents, opening new avenues for the treatment of infectious, inflammatory, and degenerative diseases.[26]

The current work focuses on the design, synthesis, and characterization of novel metal complexes derived from biologically active ligands, and evaluates their pharmacological potential, particularly their antimicrobial, antioxidant, and hemolytic activities.

2. Experimental

2.1. Materials and Instrumentation

The chemicals and solvents used in this work were purchased from various suppliers, including Sigma Aldrich, BHD, GCC, and Hi-Media. They were used without further purification. All reactions were monitored by thin-layer chromatography (TLC), and the spots were visualized by heating $KMnO_4$-stained plates. UV-Visible spectra were recorded using a Shimadzu UV-1800 UV-Vis Spectrophotometer. IR spectra were recorded as KBr disks using a SHIMADZU FTIR-8400S. ^{1}H NMR and ^{13}C NMR spectra were measured in deuterium dimethyl sulfoxide (DMSO-d6) using a Bruker Bio Spin at 400 MHz and 125 MHz, Mass spectra were recorded using an Agilent 5973 Mass Spectrometer (Agilent Technologies, USA). Melting points were determined utilizing a Stuart SMP-30 capillary melting apparatus. Magnetic susceptibility measurements were performed using a VSM MDK magnetometer, and molar conductivity was measured under standard conditions.

2.2. Methods

2.2.1. Synthesis of Imidazole-Based ligand (L)

A mixture of diketone (9,10-phenathroquinone) (1 mmol), aromatic aldehyde (2-hydroxy-5-methoxybenzaldehyde) (1 mmol), NH_4OAc, (4 mmol) was dissolved in glacial acetic acid (20 mL) and placed in 100 mL round flask, the mixture was reflexed at 120°C for (6–8) hours, and the reaction progress was detected by Thin-layer chromatography (TLC). After completion, the reaction mixture was poured into a sufficient amount of cold water, followed by the dropwise addition of ammonium hydroxide solution under stirring to precipitate the product, then the solid was filtered and thoroughly washed with deionized water to remove residual base and salts, dried, and recrystallized from ethanol **.**

2-(1H-phenanthro[9,10-d] imidazol-2-yl) phenol (L): M. p. 264–266 °C; yield 77 %. FT-IR (KBr, cm^{-1}): 3309 phenolic (OH), 3064 aromatics (C–H), 2941-2879 aliphatic (C–H), 1658 (C = N). ^{1}H NMR (400 MHz, DMSO-*d*6) δ 13.72 (s, 1H), 13.17 (s, 1H), 8.97 – 8.87 (m, 2H), 8.62 (d, *J* = 8.0 Hz, 1H), 8.52 (d, *J* = 7.9 Hz, 1H), 8.27 (dd, *J* = 8.1, 1.7 Hz, 1H), 7.80 (dt, *J* = 13.8, 7.5 Hz, 2H), 7.71 (t, *J* = 7.1 Hz, 2H), 7.41 (td, *J* = 8.4, 1.6 Hz, 1H), 7.20–7.01 (m, 2H). ^{13}C NMR (100 MHz, DMSO) δ 157.85, 149.78, 134.59, 131.58, 128.42, 128.16, 127.99, 127.80, 126.71, 126.36, 126.28, 126.12, 125.99, 124.68, 124.39, 122.66, 122.36, 122.19, 119.58, 117.67, 113.42. Anal. Calculated for C21H14N2O : C, 81.27; H, 4.55; N, 9.03. Found: C, 81.32; H, 4.45; N,9.10.

2.2.2. Synthesis of Metal Complexes (N1-N4)

Each complex was synthesized by dissolving metal salt ($FeCl_2{\cdot}4H_2O$, $CuCl_2{\cdot}2H_2O$, $NiCl_2{\cdot}6H_2O$, and $CoCl_2{\cdot}6H_2O$) in ethanol (15 mL), and mixed with a solution of imidazole ligand (2 mmol) in ethanol (20 mL). The mixture was refluxed at 75◦C with shaking for 3–5 hours. The formation of complexes was indicated by a color change and precipitation. The resulting precipitate was filtered, washed with cold ethanol, and dried; the product was purified by using the recrystallization technique.

$C_{42}H_{28}N_4O_2FeCl_2$ (N1): Yield: 67 %. ^{1}H-NMR (400 MHz, DMSO-d_6) :δ 13.77 (s, 1H), 11.19 (s, 1H), 8.90 (d, *J* = 8.2 Hz, 6H), 8.77 (s, 2H), 8.64–8.49 (m, 2H), 7.77 (d, *J* = 7.7 Hz, 5H), 7.71 (d, *J* = 7.8 Hz, 5H), 7.41 (d, *J* = 7.8 Hz, 2H), 7.13 (d, *J* = 8.1 Hz, 2H), 7.06 (d, *J* = 7.5 Hz, 2H). MS(ESI): *m/z* =747.47 [M^+].

$C_{42}H_{28}N_4O_2CuCl_2$ (N2): Yield: 76 %. ^{1}H- NMR (400 MHz, DMSO-d_6) δ 13.72 (s, 1H), 13.15 (s, 1H), 9.14

(s, 2H), 9.02 (s, 1H), 8.84 (s, 2H), 8.62 (s, 1H), 8.48 (s, 1H), 8.28 (s, 1H), 8.14–7.99 (m, 3H), 7.70 (d, *J* = 39.2 Hz, 10H), 7.36 (s, 2H), 7.05 (s, 3H). MS(ESI): *m/z* =755.05, [M^+].

$C_{42}H_{28}N_4O_2NiCl_2$ (N3): Yield: 63 %. ^{1}H-NMR (400 MHz, DMSO-d_6) :δ 13.77 (s, 1H), 11.19 (s, 1H), 8.90 (d, *J* = 8.2 Hz, 6H), 8.77 (s, 2H), 8.64 – 8.49 (m, 2H), 7.77 (d, *J* = 7.7 Hz, 5H), 7.71 (d, *J* = 7.8 Hz, 5H), 7.41 (d, *J* = 7.8 Hz, 2H), 7.13 (d, *J* = 8.1 Hz, 2H), 7.06 (d, *J* = 7.5 Hz, 2H). MS(ESI): *m/z* =755.25 [M^+].

$C_{42}H_{28}N_4O_2CoCl_2$ (N4): Yield: 84 %. ^{1}H- NMR (400 MHz, DMSO-d_6) δ 13.71 (s, 1H), 11.15 (s, 1H), 8.86 (d, J = 8.3 Hz, 4H), 8.51 (d, J = 26.3 Hz, 4H), 8.26 (d, J = 7.7 Hz, 2H), 7.76 (t, J = 7.5 Hz, 5H), 7.66 (t, J = 7.6 Hz, 4H), 7.38 (t, J = 7.7 Hz, 2H), 7.19–7.02 (m, 5H). MS(ESI): *m/z* =750.30 [M^+].

2.2.3. *In vitro* Antibacterial assay

Grow each bacterial strain overnight in the nutrient broth at 37°C. The turbidity was adjusted to the 0.5 McFarland standard (~1.5×10^8 CFU/mL) using sterile saline. Swab the adjusted bacterial suspension evenly onto MHA plates to form a lawn. Allow the plates to dry for 5–10 minutes. Use a sterile cork borer to create three wells (6 mm diameter) in each MHA plate. Add 100 µL of each sample concentration (300, 200, 100 ppm) into separate wells. Place a carbapenem on the same plate as a positive control. Incubate plates at 37 °C for 18–24 h. After incubation, measure the diameter of the inhibition zones (mm) around the well using a ruler. Measure from edge to edge (including well diameter).

2.2.4. *In vitro* antioxidant assays

A standard stock solution of DPPH was prepared by dissolving 2 mg of DPPH in 100 ml of methanol. Then, 500 μL of the DPPH solution was mixed with 100 μL of each of the tested compounds (L and N1-N4) at various concentrations, also dissolved in methanol. The mixture was incubated in the dark at room temperature for 35 minutes, and absorbance was measured at 517 nm utilizing methanol as a *T* percentage of DPPH radical inhibition activity (% Inhibition) was calculated according to Eq. (1):

$$I\,\% = (A^\circ - A_t / A^\circ) \times 100, \quad (1)$$

where $A_\circ$ is the absorbance of the DPPH solution without the sample, and A_t is the absorbance in the presence of the test compound.

The IC_{50} value, defined as the concentration of a compound required to inhibit 50 % of DPPH free radicals, was determined by plotting the percentage inhibition *versus* sample concentration. Ascorbic acid was used as a positive control for comparison.

2.2.5. *In vitro* hemolysis assays

The hemolytic activity of the synthesized compounds (**L and N1-N4**) was assessed utilizing human red blood cells (hRBCs). Fresh human blood was collected from a healthy donor into tubes containing heparin to prevent coagulation. The blood was centrifuged at 1500 rpm for 10 minutes at 4 °C to separate the plasma. The supernatant was discarded, and the RBC pellet was washed three times with sterile phosphate-buffered saline (PBS, pH 7.4) to remove plasma proteins and other residues. After washing, the RBCs were diluted with PBS to prepare a 2 % (v/v) erythrocyte suspension for the assay. The test compounds were prepared in PBS at various concentrations. For each test, 200 µL of the compound's solution was mixed with 800 µL of the RBC suspension in sterile microcentrifuge tubes. The mixture was incubated at 37 °C for 1h with occasional shaking. After incubation, the tubes were centrifuged at 1500 rpm for 10 min, and the absorbance of the supernatant was measured at 540 nm using a UV–Vis spectrophotometer to determine the release of hemoglobin as an indicator of cell lysis. PBS was used as a negative control (0%hemolysis), and 0.1 % Triton X-100 served as a positive control (100 % hemolysis). The percentage of hemolysis was calculated using the following formula:

$$\%\ \text{Hemolysis} = (A_{sample} - A_{negative\ control}) / (A_{positive\ control} - A_{negative\ control}) \times 100\ \%, \quad (2)$$

A_{sample}: The absorbance of the test solution; $A_{negative\ control}$: The absorbance of PBS; $A_{positive\ control}$: The absorbance of Triton X-100.

3. Results and Discussion

3.1. Preparation of ligand and its metal complexes

The synthetic approach adopted in this study successfully led to the formation of imidazole-based ligands and their corresponding metal complexes with various transition metal ions. The ligands were prepared *via* a condensation reaction under controlled conditions, resulting in high purity. As shown in scheme (1). The presence of key donor atoms, such as nitrogen and oxygen, within the imidazole scaffold provided suitable coordination sites for metal ions, enhancing their ability to form stable chelates. The proposed structures of the new complexes are presented in Fig. 1.

3.2. The elemental analysis and physical properties of the synthesized compounds

The metal complexes derived from the imidazole ligand were prepared in good yields by reacting imidazole with $FeCl_2{\cdot}4H_2O$, $Cu{\cdot}Cl_2{\cdot}2H_2O$, $NiCl_2{\cdot}6H_2O$, and

$CoCl_2 \cdot 6H_2O$. The successful formation of metal complexes was demonstrated by the remarkable changes in the physical properties of the products compared to the free ligand, such as changes in color, melting point, and solubility. Most of the complexes were found to be colored solids that were stable in air, with melting points above 200 °C. They exhibited low solubility in water, but were soluble in polar, aprotic solvents such as DMSO and DMF, indicating strong metal-ligand compatibility.

Elemental (C, H, N) analysis of the ligand and complexes agreed well with the calculated values, Table 1. The results also indicated a 1:2 metal-to-ligand ratio, supporting the proposed structures of these new complexes.

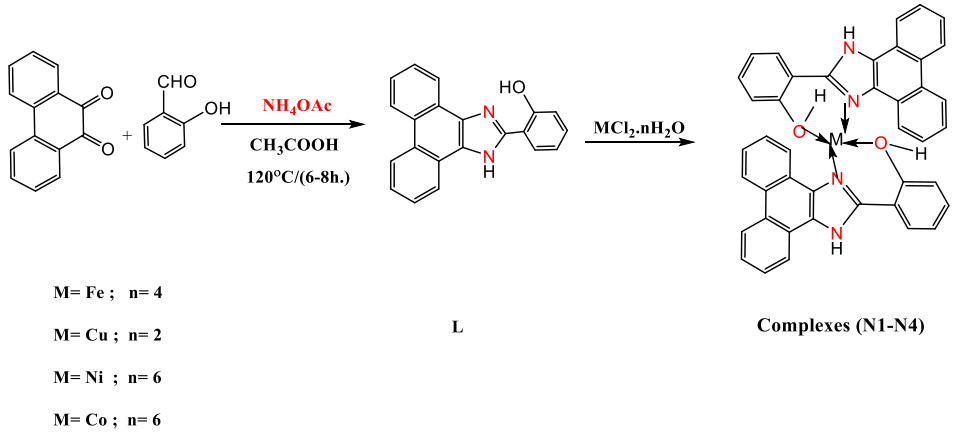

Scheme 1. Reaction scheme of Imidazole ligand L and complexes (N1-N4)

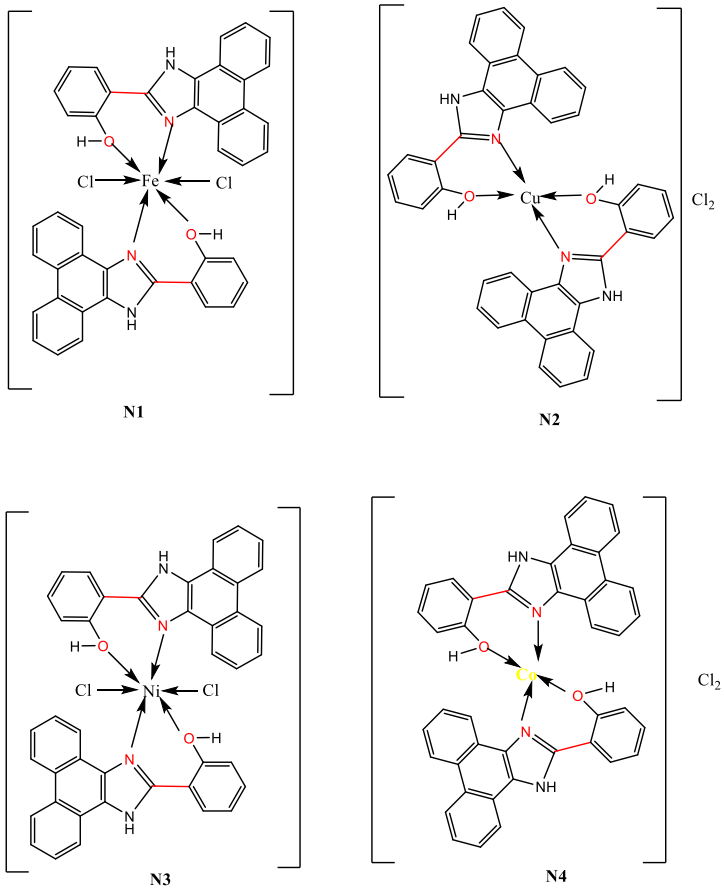

Fig. 1. Proposed structures of the newly complexes

Table 1. Physical properties and analytical data of ligand and its complexes (L and N1-N4)

Comp	Molecular Formula	M: L	M. Wt., g. mol^{-1}	Color	M.P, ^0C	Yield, %	Elemental analysis Calc. (found)			A, Ohm^1. cm^2mol^{-1}
L	$C_{21}H_{14}N_2O$	–	310.36	Brown	264–266	77	81.27 (81.11)	79.61 (79.56)	9.03 (9.11)	–
N1	$C_{42}H_{28}FeN_4O_2Cl_2$.	1:2	747.46	Yellow	252–254	67	67.49 (67.44)	3.78	7.50	13
N2	$C_{42}H_{28}CuN_4O_2CL_2$	1:2	684.26	Dark-Greenish	235–236	76	73.72 (73.70)	4.12	8.19	76
N3	$C_{42}H_{28}NiN_4O_2CL_2$	1:2	679.41	Yellow-Greenish	210–212	63	67.32 (67.29)	3.76	7.47	17
N4	$C_{42}H_{28}CoN_4O_2CL_2$	1:2	648.72	Dark-Blue	244–246	84	79.61 (79.56)	4.35	8.64	80

3.3. Infrared Spectra

The main and characteristic FT-IR bands of the ligand (Fig. 2) and its complexes (Figs. 3–6) are depicted in Table 2. The FT-IR spectral data of the ligand showed characteristic absorption bands around **3315** and 3547 cm^{-1}, which are attributed to N–H and O–H stretching, respectively,[27] and absorption bands around 1658 cm^{-1}, which correspond to C=N stretching inside the imidazole ring. As for the metal complexes, the C=N band shifted to lower wavenumbers, indicating coordination of the imidazole nitrogen to the metal center. New bands appeared in the range of 500–600 cm^{-1}, corresponding to M–N and M–O vibrations, confirming metal-ligand coordination.

Table 2. The characteristic FT-IR absorption bands of the ligand (L) and complexes (N1-N4)

Comp.	ν(N-H)	ν (O-H)	ν (C=N)	ν (C-N)	ν (M-O)	ν (M-N)
L	3465	3309	1658	1278	-	-
N1	3360	3457	1649	1257	515	430
N2	3487	3514	1651	1235	516	424
N3	3315	3547	1653	1257	553	457
N4	3425	3508	1651	1257	543	461

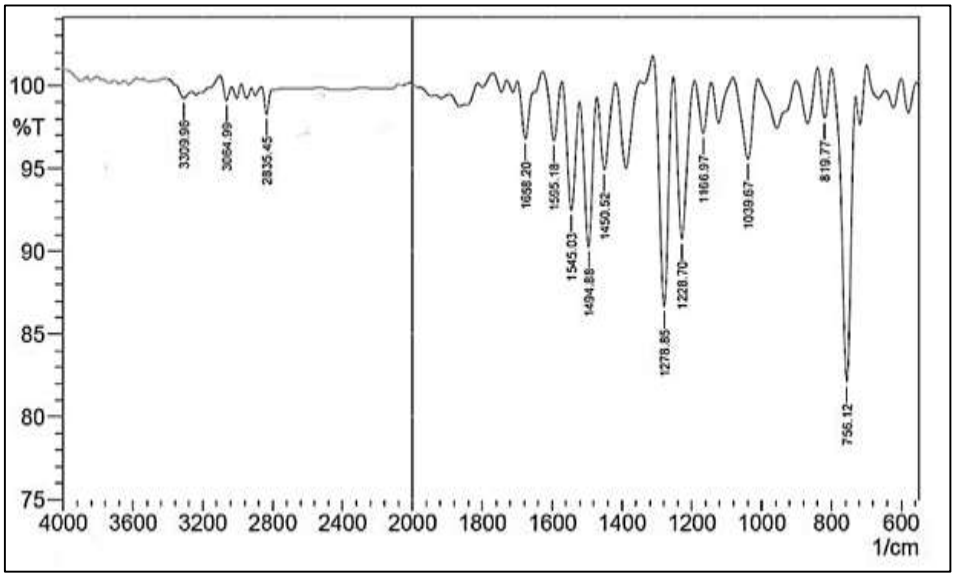

Fig. 2. FT-IR for L

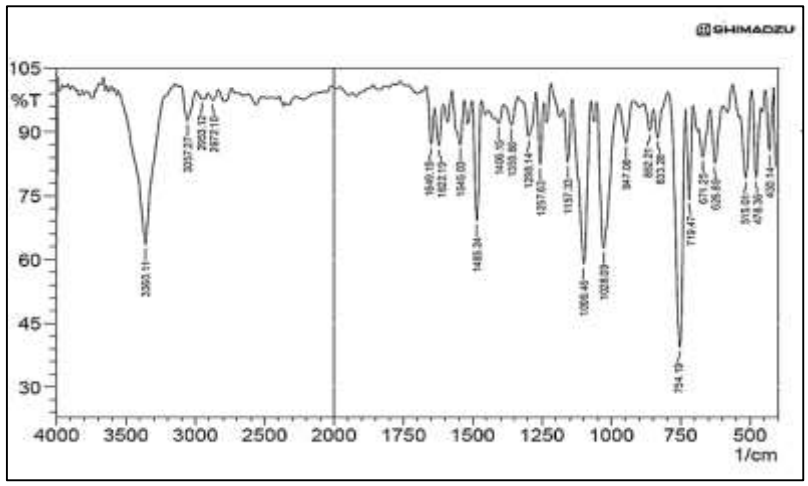

Fig. 3. FT-IR for N1

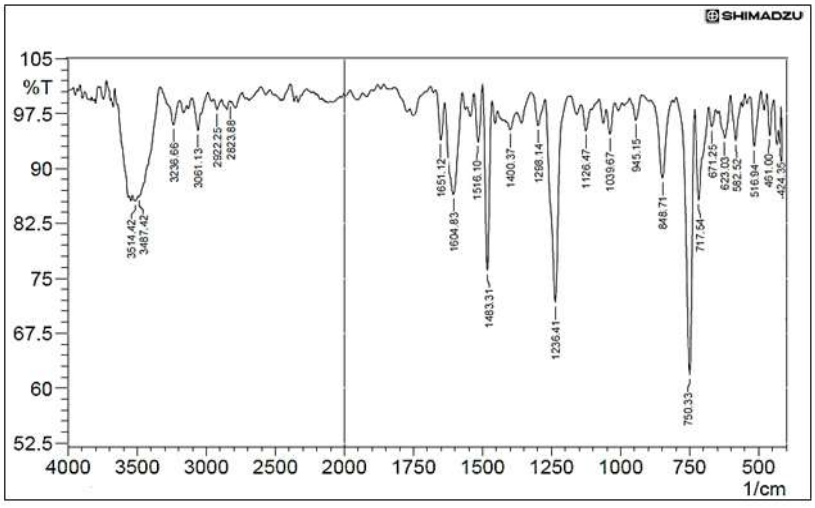

Fig. 4. FT-IR for N2

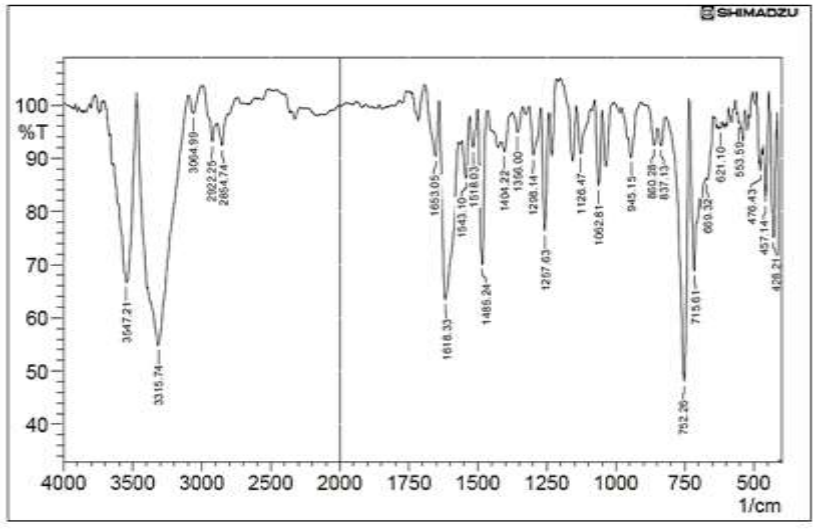

Fig. 5. FT-IR for N3

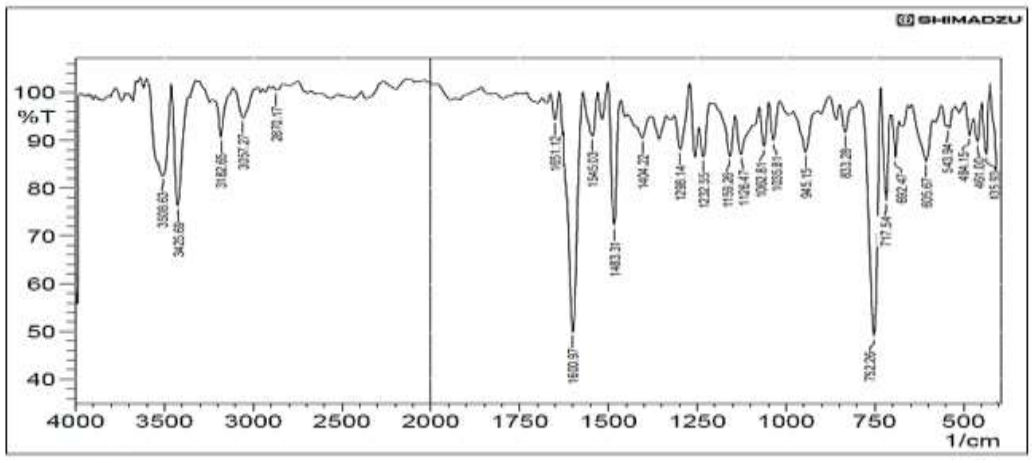

Fig. 6. FT-IR for N4

3.4. UV-Visible Spectroscopy

Table 3 shows the electronic spectra of the ligands with their complexes in ethanol at a concentration of 10^{-3} M, and Fig. 7 shows the corresponding spectra. The free ligand displayed characteristic (π→π*) and (n→π*) transitions in the UV region (typically 230–290 nm). Upon complexation, additional absorption bands were observed in the visible region (~400–700 nm), attributed to d–d transitions specific to each metal ion, confirming the formation of coordination complexes.[28]

Table 3. Electronic Spectral Data for the free ligand and metal complexes

Comp.	λ_{max}, nm	Band Assignment
L	239,368	π→π*, n→π*
N1	500	d-d / LMCT transition
N2	548	d-d / LMCT transition
N3	455	d-d / LMCT transition
N4	469	d-d / LMCT transition

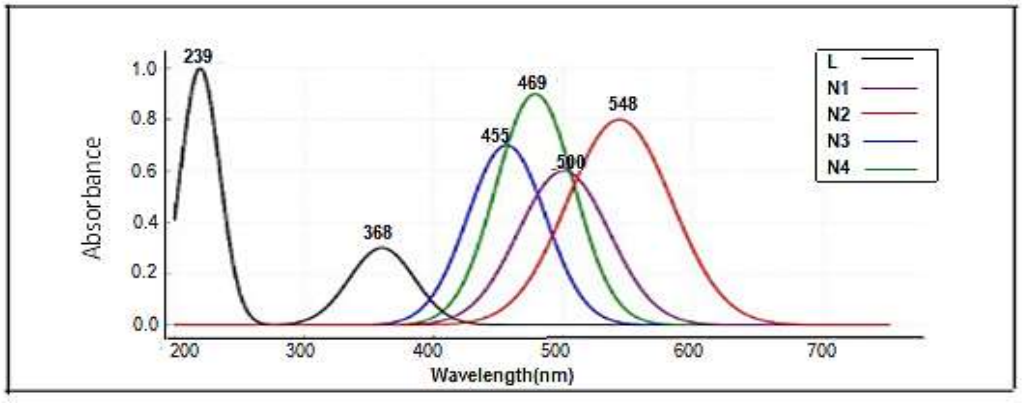

Fig. 7. UV-Visible spectra for L and N1-N4

3.5. ^{1}H-NMR spectroscopy

In the ^{1}H-NMR spectra (Figs. 8–12), the free ligand was confirmed by characteristic signals in the range (8.94–7.09) ppm, which correspond to aromatic protons; the N-H signal appeared as a singlet 13.72 ppm, and a singlet at 13.17 ppm was observed and assigned to the phenolic OH. In the metal complexes, slight shifts and broadening of signals were observed, suggesting ligand-metal ions interaction, which alters the electronic environment**.** The spectral data of all complexes are detailed in the experimental part.

The ^{1}H NMR spectrum of N3. The ^{1}H-NMR spectrum did not exhibit any observable proton signals. This absence can be attributed to the strong paramagnetic nature of the Ni (II) center, which induces rapid nuclear spin relaxation. As a result, the proton resonances become extremely broadened and diminished in intensity, rendering them undetectable.[29]

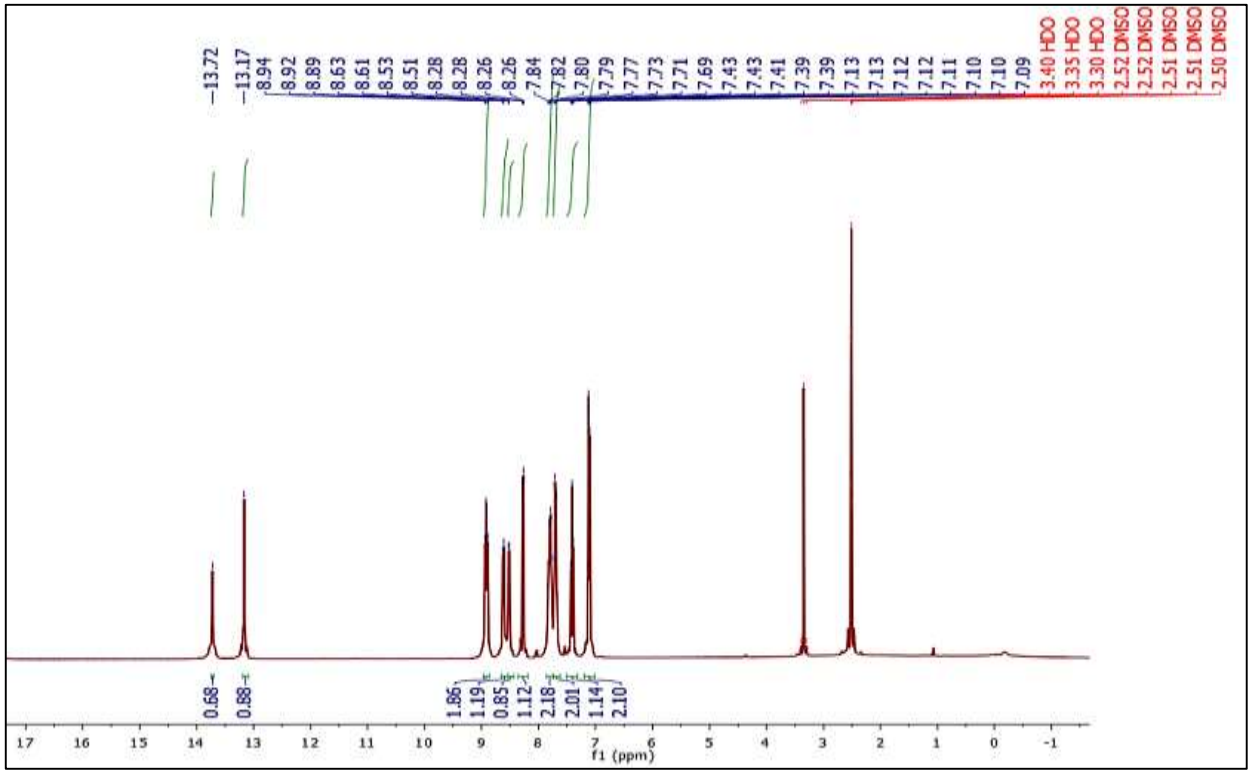

Fig. 8. [1]HNMR of L (DMSOd6, 400 MHz)

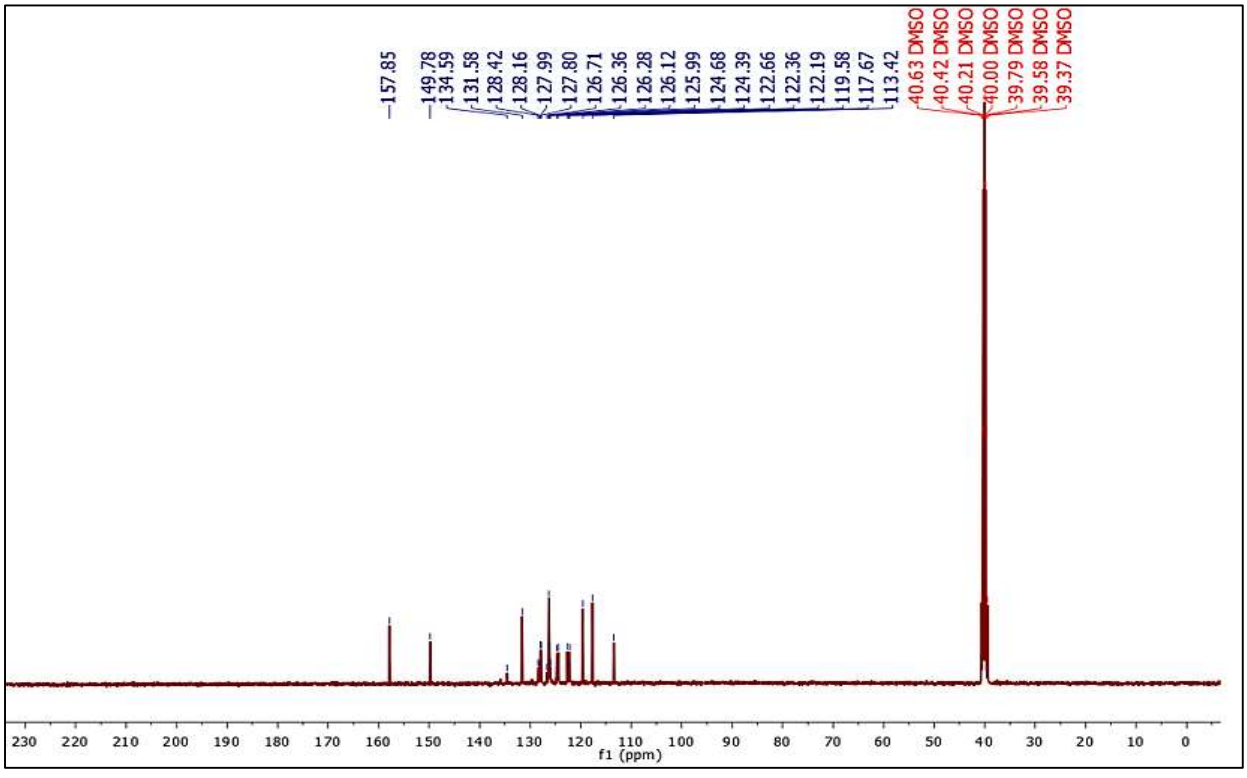

Fig. 9. [13]CNMR of L (DMSO$_6$, 400 MHz)

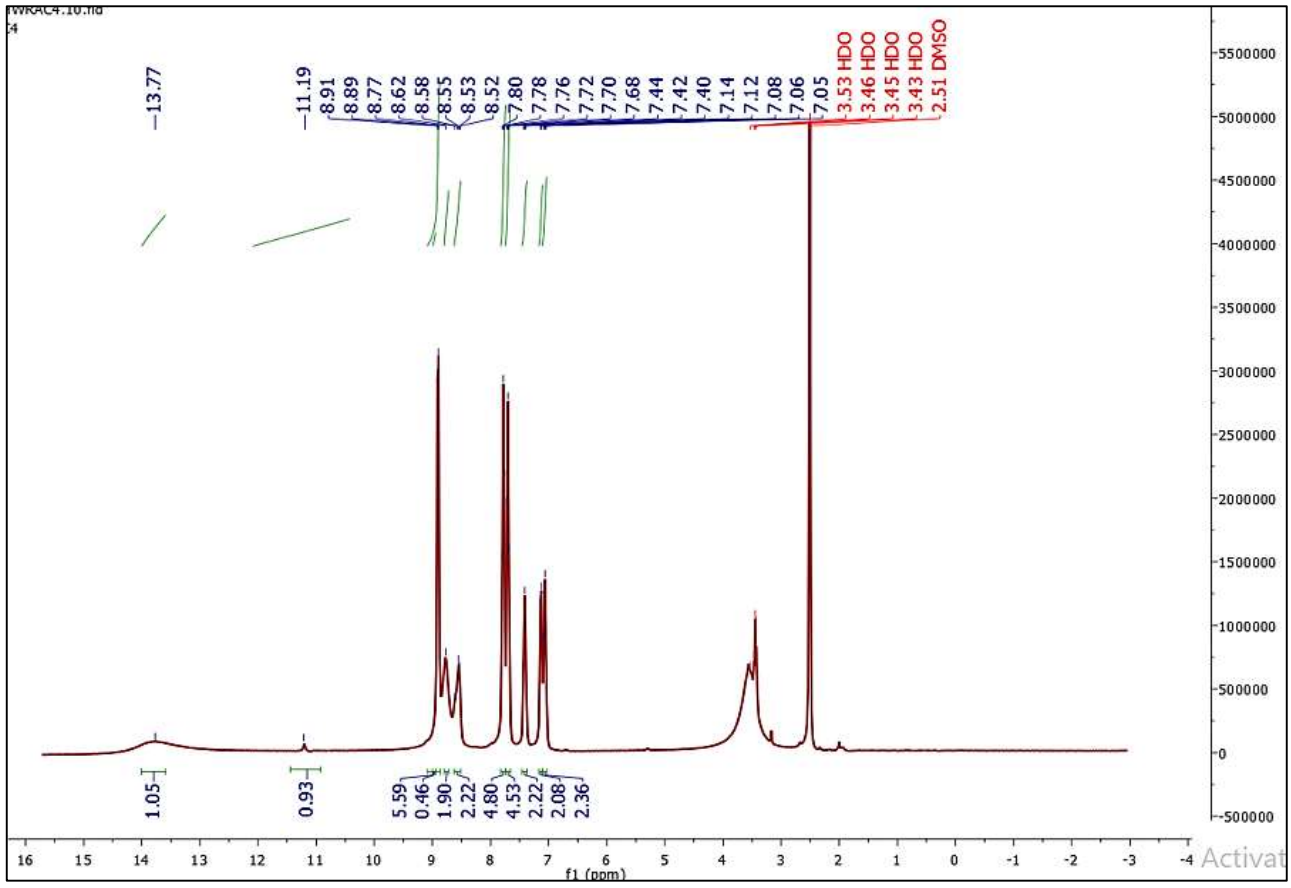

Fig. 10. [1]HNMR of N1 (DMSOd6, 400 MHz)

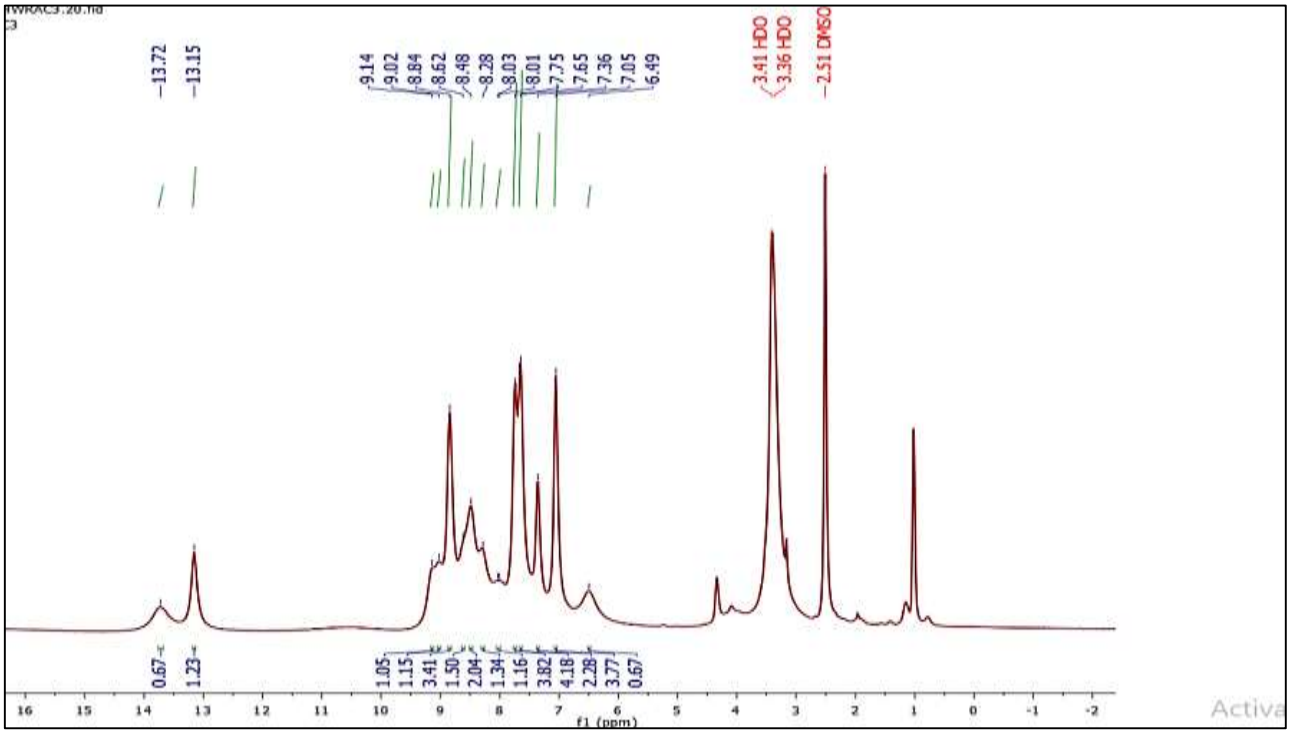

Fig. 11. [1]HNMR of N2 ($DMSOd_6$, 400 MHz)

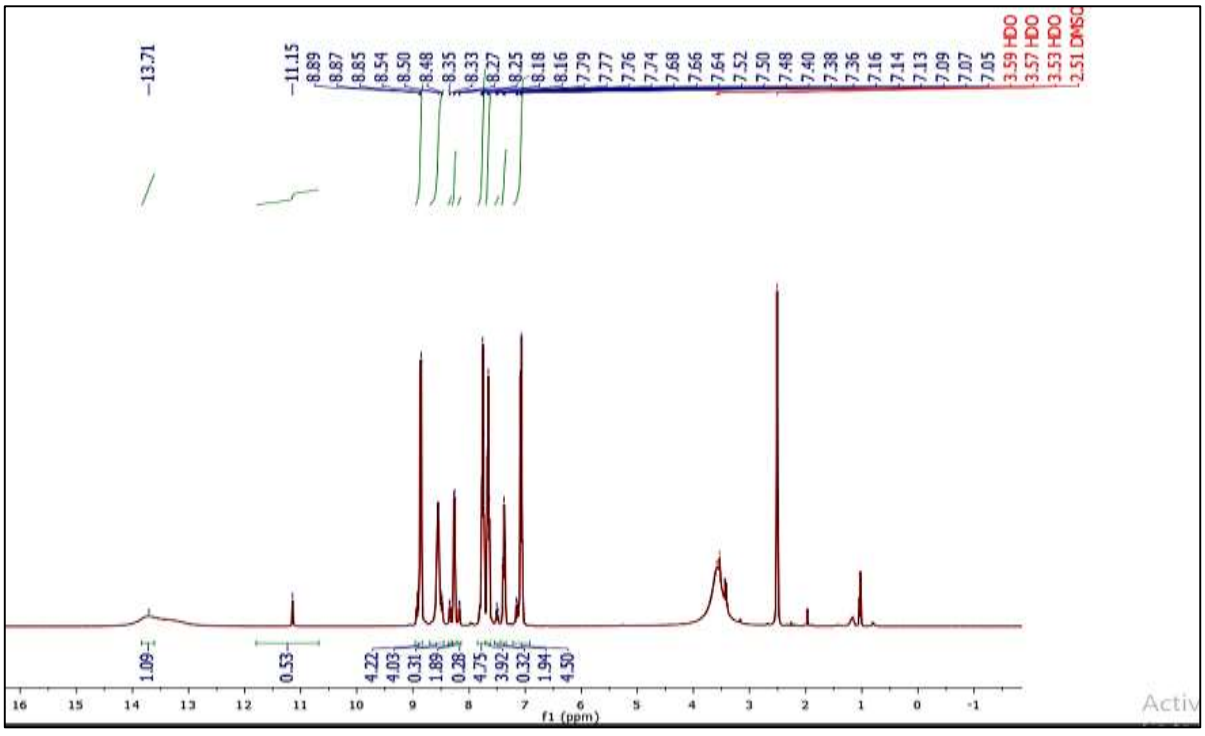

Fig. 12. ^{1}HNMR of N4 (DMSOd_6, 400 MHz)

3.6. Mass Spectra of the Metal Complexes

The mass spectra of the complexes (Figs. 13–16) confirmed their proposed molecular formulas. The spectra of the complexes (Figures) showed molecular ion peaks at m/z 747.47, 755.05, 755.25, and 750.30 for N1, N2, N3, and N4, respectively. These values are consistent with the calculated molecular weights from elemental analysis (Table 1), supporting the suggested structures.

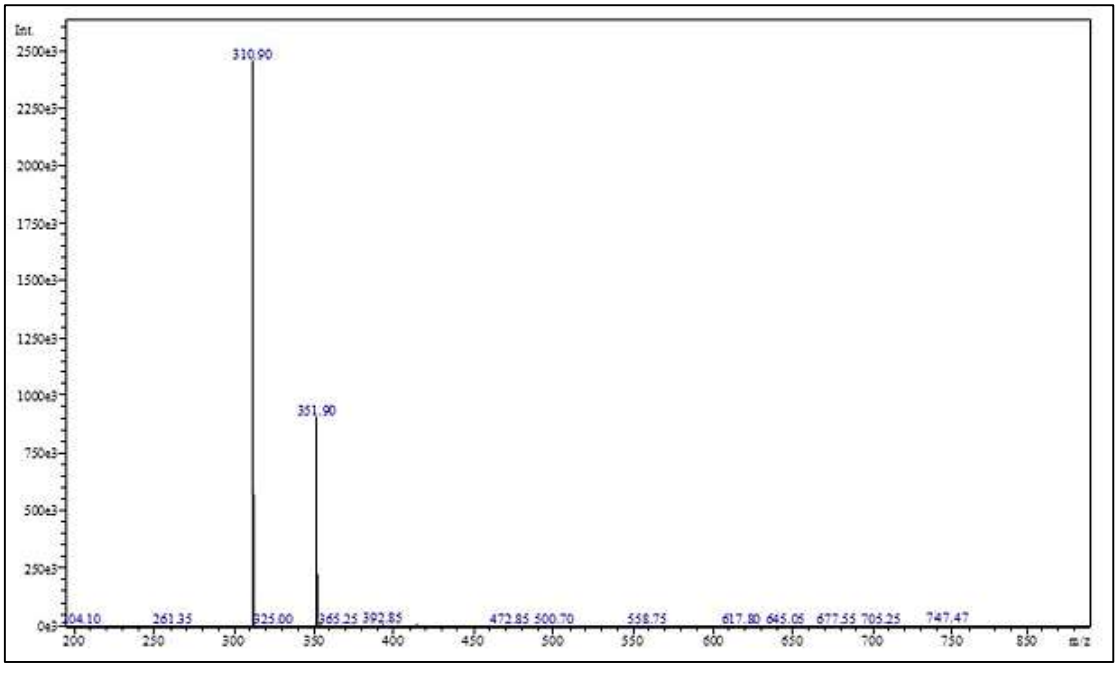

Fig. 13. Mass Spectra of N1

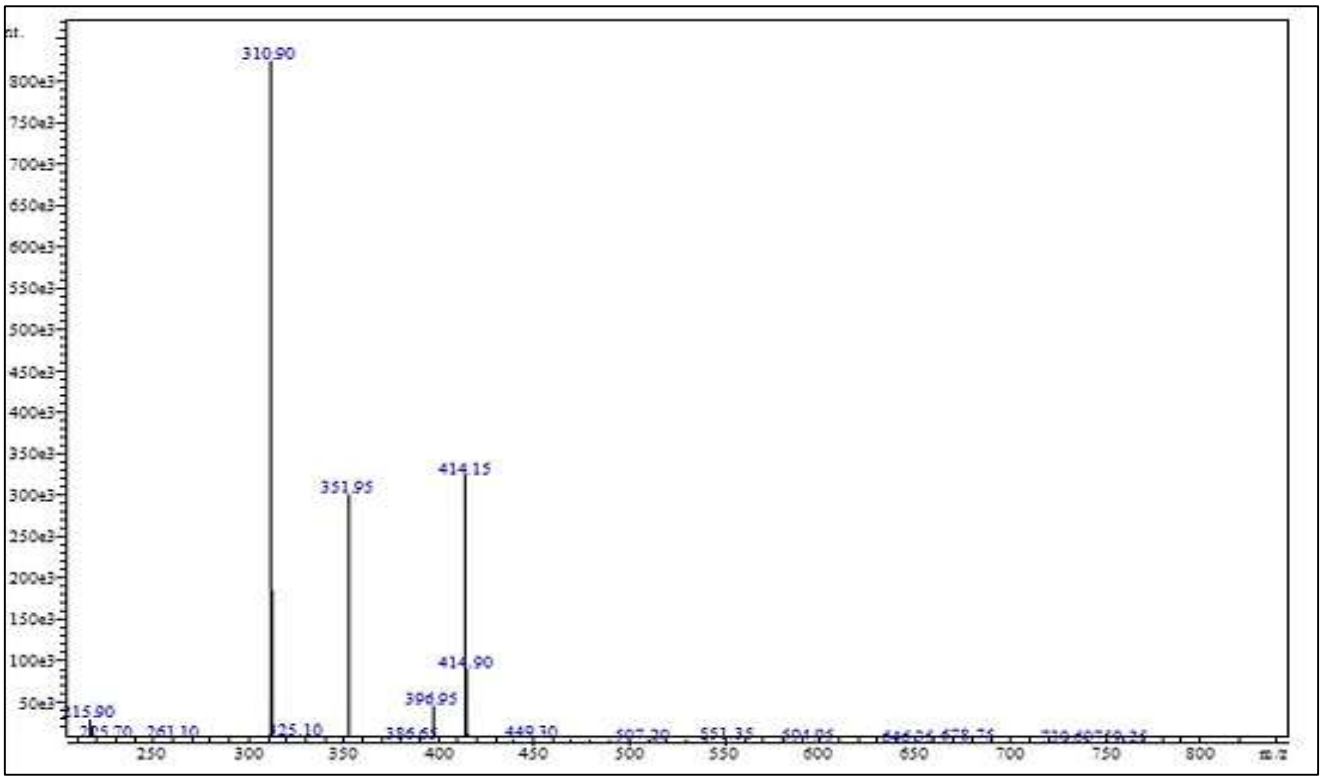

Fig. 14. Mass Spectra of N2

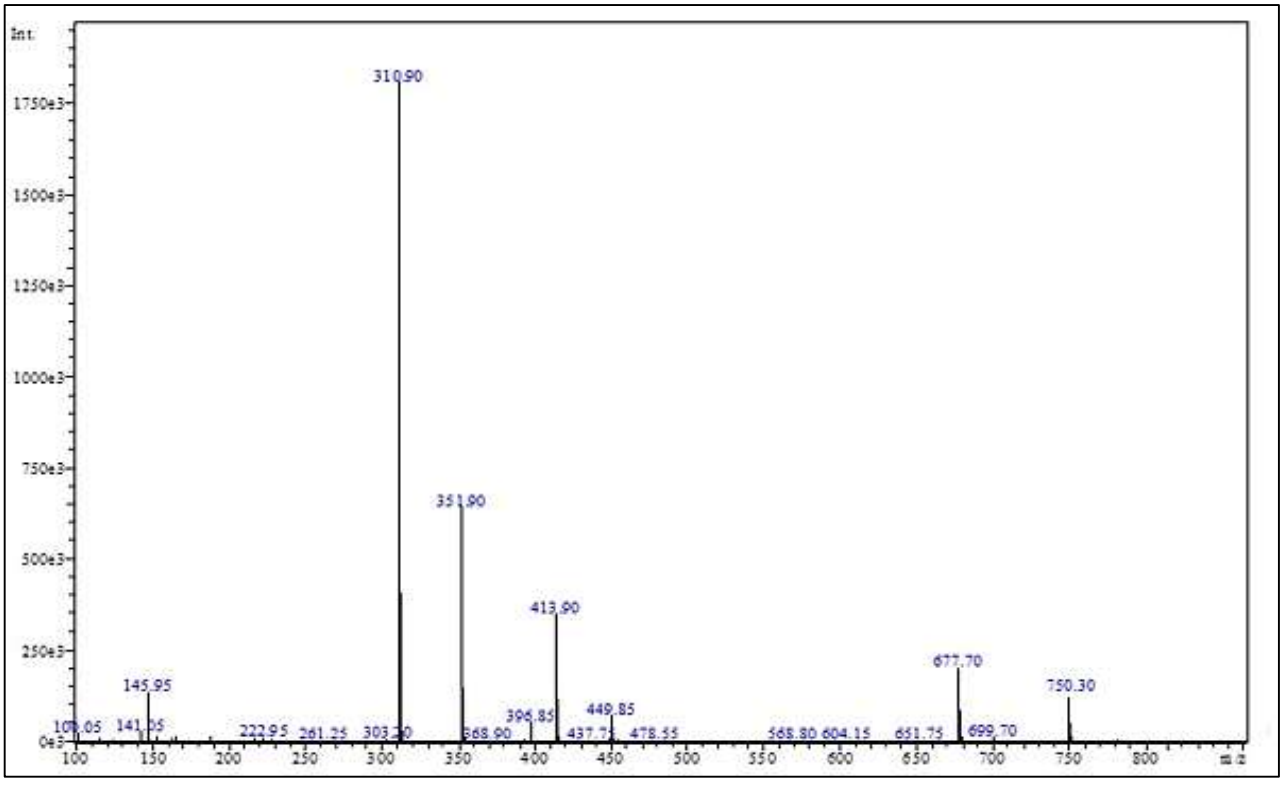

Fig. 15. Mass spectra of N3

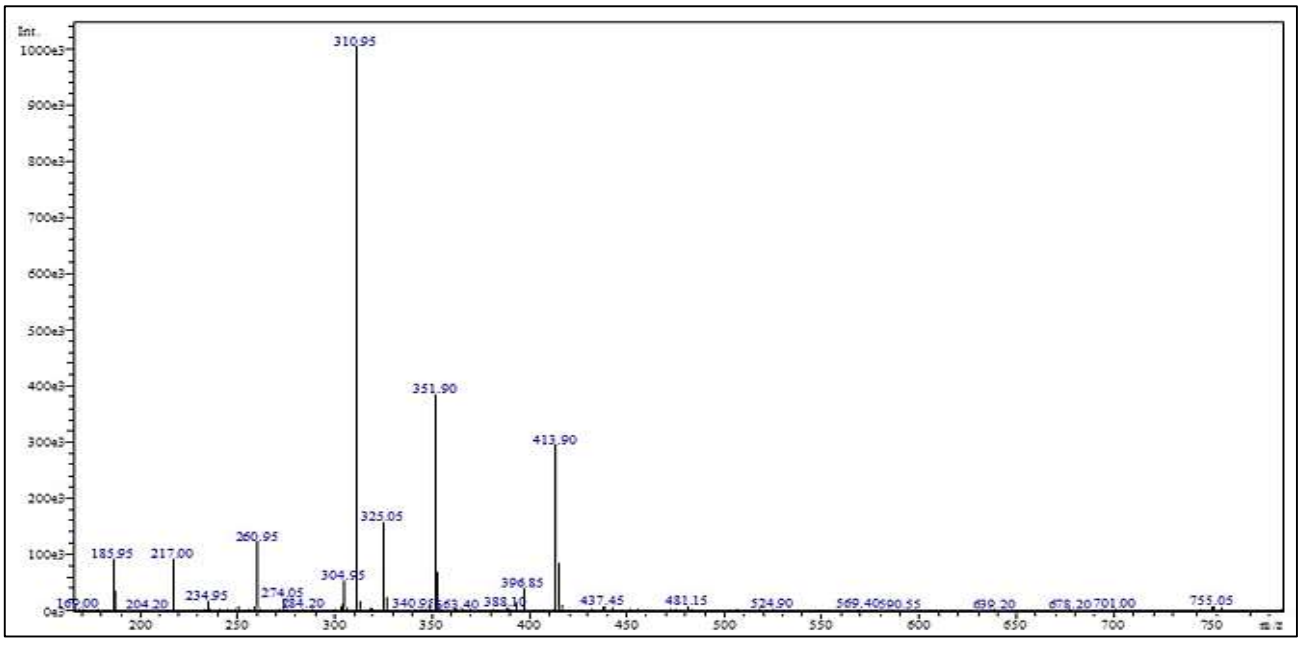

Fig. 16. Mass Spectra of N4

3.7. Magnetic Susceptibility Measurement

Magnetic susceptibility is an important diagnostic tool in inorganic chemistry that can be used to suggest the spatial shapes of transition metal complexes. It relies primarily on the effects resulting from the occupancy of electrons in partially filled outer electron shells. These measurements are used to determine the number of unpaired electrons, thus determining whether the complex under study has high or low spin. A metallic complex is classified as paramagnetic when the central atom contains unpaired electrons, while diamagnetic when these unpaired electrons are paired.30

The magnetic moment values were measured using the Miran-Coy method for the complexes, and it was found that they possess magnetic properties using the following equations:

$$\mu_{S+L}=2\sqrt{S(S+1)} \quad \text{B.M}$$

Magnetic susceptibility measurements for the N1 recorded a magnetic moment of 1.21 B.M (diamagnetic). This is consistent with the moments of iron (II) complexes with an octahedral shape. Magnetic susceptibility measurements for the N2 have a magnetic moment of 4.51 B.M (paramagnetic), respectively. This is attributed to the presence of only one unpaired electron in the d^9 system. The results for N3 showed that it has a magnetic moment of 4.35 B.M., which is consistent with the recorded measurements. Regarding the magnetic moment values for octahedral nickel complexes, this clearly indicates the presence of paramagnetic properties due to the presence of two lone electrons in the (d^8) system. Magnetic susceptibility measurements for the N4 recorded a magnetic moment of 4.28 B.M (paramagnetic). This is consistent with the moments of cobalt complexes with a tetrahedral shape.

3.8. Antibacterial Activity

The ligand and its complexes were tested for antibacterial activity against four types of micro-organisms: two Gram-positive (*Staphylococcus aureus* and *Streptococcus pyognenes*) and two Gram-negative (*Escherichia coli* and *Pseudomonas aerogeza*) bacteria, using the disc diffusion method and measured as zone of inhibition (mm) at three concentrations of 100, 200, 300 µg/mL. As depicted in Table (4) and Figs. 17 and 18, the free ligand L showed good activity with inhibition zones ranging from 26–40 mm, comparable to the standard drug Carbenicillin.

The metal complexes showed variable inhibition zones against *Staphylococcus aureus*. and *Escherichia coli*, with the highest activity against *Staphylococcus aureus* observed for N3and N4 complexes, and against *E. coli*, the highest inhibitory effect was reported for the N2 and N4 complexes, respectively, with inhibition zones ranging from 10–31 mm. On the other hand, L and all metal complexes do not exhibit any activity against *Streptococcus pyognenes* and *Pseudomonas aerogeza* bacteria except for Carbenicillin. Metal complexation enhances antimicrobial properties, likely due to improved lipophilicity or membrane permeability.[31]

Table 4. Antibacterial activity of free ligand (L) and its complexes (N1–N4)

Sample	Zone of inhibition (mm)											
	Staphylococcus aureus			*Streptococcus pyognenes*			*Pseudomonas aerogeza*			*Escherichia coli*		
	Conc., μg/mL			Conc., μg/mL			Conc., μg/mL			Conc., μg/mL		
	100	200	300	100	200	300	100	200	300	100	200	300
L	26	33	40	0.0	0.0	0.0	0.0	0.0	0.0	17	18	15
N1	10	20	26	0.0	0.0	0.0	0.0	0.0	0.0	8	11	13
N2	21	24	28	0.0	0.0	0.0	0.0	0.0	0.0	14	17	20
N3	20	26	31	0.0	0.0	0.0	0.0	0.0	0.0	10	15	18
N4	18	25	30	0.0	0.0	0.0	0.0	0.0	0.0	19	20	19
Carbenicillin	35	36	37	25	26	30	28	25	27	27	25	29
DMSO	0.0	0.0	0.0	0.0	0.0	0.0	0.0	0.0	0.0	0.0	0.0	0.0

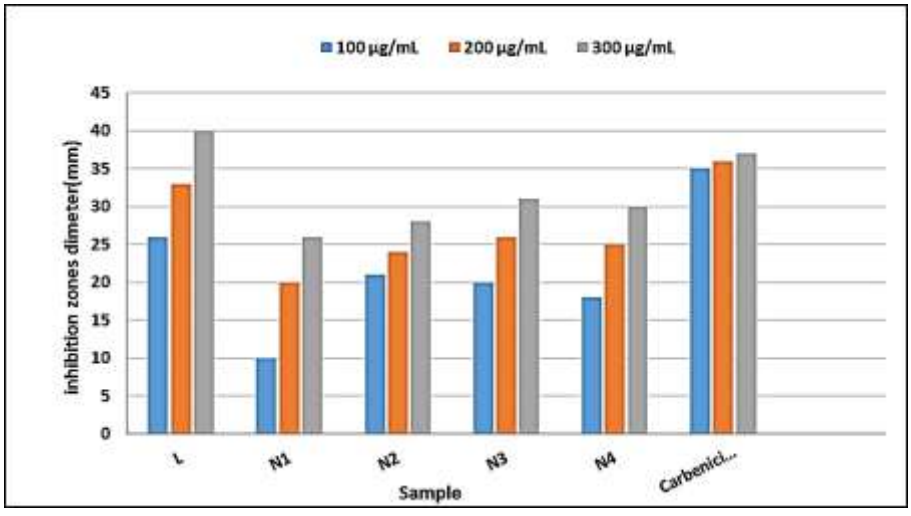

Fig. 17. The inhibitory activity of the synthesized compounds against ***Staphylococcus aureus***

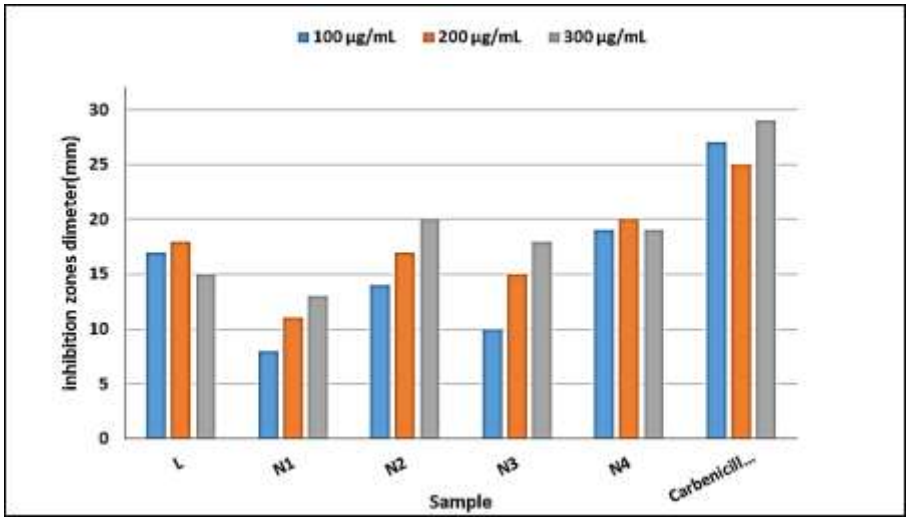

Fig. 18. The inhibitory activity of the synthesized compounds against ***Escherichia Coli***

3.9. Antioxidant Activity

Antioxidants are biologically active species, capable of scavenging free radicals associated with diseases, like cancer.[32] Their structures contain mobile protons (*e. g.,* ***OH, NH***, ...), enabling them to directly scavenge reactive oxygen species (ROS)**.**

The ability of the free ligand and its complexes to scavenge free radicals was assessed by various concentrations (100–500 µg/mL) utilizing UV–Vis spectroscopy and compared to the antioxidant ascorbic acid. The antioxidant activity increases with concentration in all cases, indicating a dose-dependent response. As depicted in Table 5, all compounds exhibited antioxidant activity, although lower than that of ascorbic acid. Among complexes, N2 displayed the highest activity, but it was still lower than the reference ascorbic acid. This promising activity is likely due to the hydroxyl group, which is known to be responsible for DPPH scavenging.[33] In fact, many studies[34] have demonstrated a link between antiradical properties and the ability of antioxidants to transfer the H-atom of the OH group to free radicals, following a proposed three-step mechanism illustrated below.[35]

$$RXH + DPPH^{\bullet} \longrightarrow RXH^{\bullet+} + DPPH^{-}$$
$$RXH^{\bullet+} \longrightarrow RX^{\bullet} + H^{+}$$
$$DPPH^{-} + H^{+} \longrightarrow DPPHH$$

Table 5. DPPH radical scavenging activity of L and (N1-N4)

Comp.	Concentration, µg/m**L**					
	100	200	300	400	500	IC50
L	35.41	44.18	52.83	59.64	66.33	278.39
N1	41.07	43.83	51.13	63.14	72.6	265.01
N2	58.91	68.72	76.3	84.23	90.51	56.20
N3	33.60	37.01	49.83	71.42	83.27	262.95
N4	54.2	63.4	71.5	79.3	86.7	93.04
Ascorbic Acid	59.83	68.34	77.66	88.21	97.82	3.99

3.10. Hemolytic Activity (Cytocompatibility)

Hemolytic activity was evaluated by exposing human red blood cells (hRBCs) to the synthesized compounds and measuring hemoglobin release at concentrations of 100, 200, 300, 400, and 500 µg/mL (Table 6 and Fig. 19). The hemolysis assay revealed that the free ligand (L) caused higher hemolytic activity compared with its metal complexes, reaching 8.97 % at 500 µg/mL, which exceeds the acceptable limit of 5 %. This indicates that the free ligand may exert some damaging effect on the erythrocyte membrane at higher concentrations. In contrast, all metal complexes (N1, N2, N3, and N4) exhibited markedly lower hemolysis percentages, remaining below 5 % even at the maximum tested concentration. These findings suggest that coordination of the ligand with metal ions significantly improves its biocompatibility and reduces its cytotoxic interaction with red blood cells. Among the complexes, the N2 derivative demonstrated the lowest hemolytic effect, highlighting its safety and potential as a biologically compatible compound. Therefore, while the free ligand shows mild hemolytic risk at elevated doses, all metal complexes can be regarded as non-hemolytic and safe according to the 5 % threshold.[34] The positive control (Triton X-100) produced nearly complete hemolysis (95.71 %), while the negative control induced only 0.53 % hemolysis, confirming the validity of the assay. Furthermore, the dose-dependent increase in hemolysis observed for both the ligand and its complexes is consistent with concentration-related cytotoxic responses.

Table 6. Hemolytic activity of Ligand and its complexes, % hemolysis

Comp.	Concentration, µg/m**L**				
	100	200	300	400	500
L	4.09	6.07	7.65	8.39	8.97
N1	0.97	1.15	1.84	2.66	3.52
N2	1.71	2.15	2.43	2.57	2.71
N3	1.03	1.33	1.89	2.63	3.14
N4	1.13	1.36	1.65	2.64	2.93

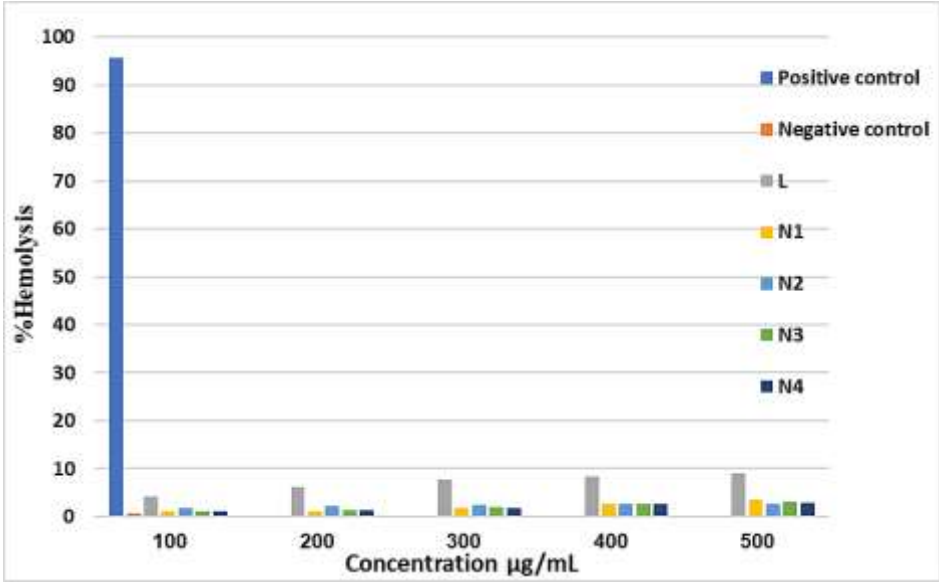

Fig. 19. Hemolytic activity of L, N1, N2, N3 and N4

4. Conclusions

In this study, a multi-substituted imidazole ligand, 2-(1H-phenanthro[9,10-d] imidazol-2-yl) phenol, and its complexes with transition metal ions Fe (II), Cu (II), Ni (II), and Co (II) were successfully prepared and characterized using various spectroscopic techniques, magnetic and elemental analysis. These results supported the success of the ligand-metal coordination process. Biological evaluation revealed that both the ligand and its metal complexes demonstrated promising antibacterial and antioxidant activities, with the metal complexes generally showing superior performance compared to the free ligand and standard drugs. Specifically, the N4 metal complex showed the most promising antimicrobial activity, displaying the highest inhibition zones against both Staphylococcus aureus and Escherichia coli, making it the most potent candidate for further biological investigations. The N2 complex demonstrated the highest antioxidant (radical scavenging) activity among the tested complexes; however, its activity remained lower than the reference standard, ascorbic acid. Hemolytic assays indicated that all compounds exhibited low to moderate toxicity toward red blood cells, suggesting acceptable biocompatibility. Therefore, it can be concluded that the prepared ligand and its complexes are promising in terms of their biological properties and may serve as a basis for the development of future pharmaceuticals and potential medical applications.

Acknowledgements

I extend my sincere thanks and gratitude to the University of Karbala – College of Science for providing a stimulating and supportive academic environment, and for the capabilities and facilities.

References

[1] Jeenat, A.; Ruby, A.; Chandrabhan, V. Imidazole and its derivatives as corrosion inhibitors. In *Organic Corrosion Inhibitors: Synthesis, Characterization, Mechanism, and Applications*; Wiley, 2021; pp 95–122. https://doi.org/10.1002/9781119794516.ch6

[2] Liu, H.; Yang, Ch.; Li, T.; Ma, S.; Wang, P.; Wang, G.; Su, Sh.; Ding, Y.; Yang, L.; Zhou, X.; *et al*. Design, Synthesis and Bioactivity Evaluation of Novel 2-(Pyrazol-4-yl)-1,3,4-oxadiazoles Containing an Imidazole Fragment as Antibacterial Agents. *Molecules* **2023**, *28*, 2442. https://doi.org/10.3390/molecules28062442

[3] Gujjarapp, R.; Kabi, A. K.; Sravani, S.; Garg, A.; Vodnala, N.; Tyagi, U.; Kaldhi, D.; Velayutham, R.; Singh, V.; Gupta, S.; *et al*. Overview on Biological Activities of Imidazole Derivatives. In *Nanostructured Biomaterials. Materials Horizons: From Nature to Nanomaterials*; Swain, B.P., Ed.; Springer: Singapore, 2022; pp. 135–227. https://doi.org/10.1007/978-981-16-8399-2_6

[4] Kedimar, N.; Rao, P.; Rao, S. A. Imidazole-Based Ionic Liquid as Sustainable Green Inhibitor for Corrosion Control of Steel Alloys: A Review. *J. Mol. Liq*. **2024**, *411*, 125789. https://doi.org/10.1016/j.molliq.2024.125789

[5] Tolomeu, H. V.; Fraga, C. A. M. Imidazole: Synthesis, Functionalization and Physicochemical Properties of a Privileged Structure in Medicinal Chemistry. *Molecules* **2023**, *28*, 838. https://doi.org/10.3390/molecules28020838

[6] Siwach, A.; Verma, P. K. Synthesis and Therapeutic Potential of Imidazole Containing Compounds. *BMC Chemistry* **2021**, *15*, 12. https://doi.org/10.1186/s13065-020-00730-1

[7] Sağlık, B. N.; Işık, A.; Çevik, U. A.; Özkay, Y. Synthesis, Characterization, and Molecular Docking Study of Some Novel Imidazole Derivatives as Potential Antifungal Agents. *J. Heterocycl. Chem*. **2018**, *56*, 142–152. https://doi.org/10.1002/jhet.3388

[8] Sawsan, K. A.; Mohammed, T. J.; Hayder, R. A., Alanood, A. A. Synthesis, Antibacterial Evaluation and molecular docking of 2,4,5-Tri-imidazole Derivatives. *Mor. J. Chem*. **2024**, *12*, 1222–1239. https://doi.org/10.48317/IMIST.PRSM/morjchem-v12i3.48221
[9] Li, Z.; Bhowmik, S.; Sagresti, L.; Brancato, G.; Smith, M.; Benson, D. E.; Li, P.; Merz, K. M., Jr. Simulating Metal-Imidazole Complexes. *J. Chem. Theory Comput*. **2024**, *20*, 6706–6716. https://doi.org/10.1021/acs.jctc.4c00581
[10] Taheri, B.; Taghavi, M.; Zarei, M.; Chamkouri, N.; Mojaddami, A. Imidazole and Carbazole Derivatives as Potential Anticancer Agents: Molecular Docking Studies and Cytotoxic Activity Evaluation. *Bull. Chem. Soc. Ethiop*. **2020**, *34*, 235–246. https://doi.org/10.4314/bcse.v34i2.14
[11] Serdaliyeva, D.; Nurgozhin, T.; Satbayeva, E.; Khayitova, M.; Seitaliyeva, A.; Ananyeva, L. Review of Pharmacological Effects of Imidazole Derivatives. *J. Clin. Med. Kazakh*. **2022**, *19*, 11–15. https://doi.org/10.23950/jcmk/12117
[12] Bouchal, B.; Abrigach, F.; Takfaoui, A.; Ichou, F.; Kabouche, Z.; Kabouche, A.; Bendahou, M. Identification of Novel Antifungal Agents: Antimicrobial Evaluation, SAR, ADME-Tox and Molecular Docking Studies of a Series of Imidazole Derivatives. *BMC Chem*. **2019**, *13*, 100. https://doi.org/10.1186/s13065-019-0623-6
[13] Sawsan, K. A; Lamyaa, S. M.; Jihan, H. A. Synthesis and Biological Evaluation of New 2,4,5-Trisubstituted and 1,2,4,5-Tetrasubstituted Imidazole Derivatives as Antioxidant and Antimicrobial Agents. *Chem. Data Collect.* **2025**, *58*, 101194. https://doi.org/10.1016/j.cdc.2025.101194
[14] Patel, H. M.; Noolvi, M. N.; Sethi, N. S.; Gadad, A. K.; Cameotra, S. S. Synthesis and Antitubercular Evaluation of Imidazo[2,1-b][1,3,4]thiadiazole Derivatives. *Arab. J. Chem*. **2013**, *10*, 717–724. https://doi.org/10.1016/j.arabjc.2013.01.001
[15] Selwin Joseyphus, R.; Reshma, R.; Arish, D.; Elumalai, V. Antimicrobial, Photocatalytic Action and Molecular Docking Studies of Imidazole-Based Schiff Base Complexes. *Results Chem.* **2022**, *4*, 100583. https://doi.org/10.1016/j.rechem.2022.100583
[16] Volpi, G.; Laurenti, E.; Rabezzana, R. Imidazopyridine Family: Versatile and Promising Heterocyclic Skeletons for Different Applications. *Molecules* **2024**, *29*, 2668. https://doi.org/10.3390/molecules29112668
[17] Hiremath, A. F.; Pradeep Kumar, M. R.; Rajagopal, K.; Barua, R.; Rab, S. O.; Alshehri, M. A.; Bin Emran, T. Imidazole-Based Metal Complex Derivatives: A Comprehensive Overview of Synthesis and Biological Applications. *Med. Chem*. **2024**, *31*, 1015–1050. https://doi.org/10.2174/0115734064332208241015154509
[18] Loginova, N. V.; Harbatsevich, H. I.; Osipovich, N. P.; Ksendzova, G. A.; Koval'chuk, T. V.; Polozov, G. I. Metal Complexes as Promising Agents for Biomedical Applications. *Curr Med Chem.* **2020**, *27*, 5213–5249. https://doi.org/10.2174/0929867326666190417143533
[19] Ndagi, U.; Mhlongo, N.; Soliman, M. E. Metal Complexes in Cancer Therapy – An Update from Drug Design Perspective. *Drug Des. Devel. Ther*. **2017**, *11*, 599–616. https://doi.org/10.2147/DDDT.S119488
[20] Lateef, H. M. A.; El-Dabea, T.; Khalaf, M. M.; Abu-Dief, A. M. Recent Overview of Potent Antioxidant Activity of Coordination Compounds. *Antioxidants* **2023**, *12*, 213. https://doi.org/10.3390/antiox12020213
[21] Boros, P.; Dyson, P. J.; Gasser, G. Classification of Metal-Based Drugs according to Their Mechanisms of Action. *Chem* **2020**, 6, 41–60. https://doi.org/10.1016/j.chempr.2019.10.013
[22] Mondal, R.; Guin, A.K.; Chakraborty, G.; Paul, N. D. Metal-Ligand Cooperative Approaches in Homogeneous Catalysis Using Transition Metal Complex Catalysts of Redox Noninnocent Ligands. *Org. Biomol. Chem*. **2022**, *20*, 296–328. https://doi.org/10.1039/D1OB01153G
[23] Gulcin, İ.; Alwasel, S. H. Metal Ions, Metal Chelators and Metal Chelating Assay as Antioxidant Method. *Processes* **2022**, *10*, 132. https://doi.org/10.3390/pr10010132
[24] Sánchez-López, E.; Gomes, D.; Esteruelas, G.; Bonafé, F.; Cianciosi, D.; Estrela, J. M.; Espinosa, A.; Ettcheto, M.; Cano, A.; López-Torres, M.; *et al*. Metal-Based Nanoparticles as Antimicrobial Agents: An Overview. *Nanomaterials* **2020**, *10*, 292. https://doi.org/10.3390/nano10020292
[25] Gautam, S.; Das, D. K.; Kaur, J. Transition Metal-Based Nanoparticles as Potential Antimicrobial Agents: Recent Advancements, Mechanistic, Challenges, and Future Prospects. *Nanoscale Res. Lett.* **2023**, *18*, 261. https://doi.org/10.1186/s11671-023-03861-1
[26] Nguyen, V.-T.; Huynh, T.-K.-C.; Gia-Thien-Thanh Ho, G.-T.-C.; Nguyen, T.-H.-A.; Dao, D. Q.; Mai, T. V. T.; Huynh, L. K.; Hoang, T. K. D. Metal Complexes of Benzimidazole-Derived as Potential Anti-Cancer Agents: Synthesis, Characterization, Combined Experimental and Computational Studies. *R. Soc. Open Sci* **2022**, *9*, 220659. https://doi.org/10.1098/rsos.220659
[27] Silverstein, R. M.; Webster, F. X.; Kiemle, D. J. *Spectrometric Identification of Organic Compounds*, 8th ed.; Wiley: Hoboken, NJ, 2014.
[28] Nourah, A.; Abd El-Lateef, H. M.; Mohamed, M.; Khalaf, M. M.; Abdou, A. Fe(III) and Ni(II) Imidazole-Benzimidazole Mixed-Ligand Complexes: Synthesis, Structural Characterization, Molecular Docking, DFT Studies, and Evaluation of Antimicrobial and Anti-Inflammatory Activities. *Dalton Trans*. **2025**, *54*, 12345–12360. https://doi.org/10.1039/D5DT00551E
[29] Ravera, E.; Gigli, L.; Czarniecki, B.; Lang, L.; Kümmerle, R.; Parigi, G.; Piccioli, M.; Neese, F.; Luchinat, C. A Quantum Chemistry View on Two Archetypical Paramagnetic Pentacoordinate Nickel (II) Complexes Offers a Fresh Look on Their NMR Spectra. *Inorg. Chem.* **2021**, *60*, 2068–2075. https://doi.org/10.1021/acs.inorgchem.0c03635
[30] Bera, R.; Ansari, M.; Alam, A.; Das, N. Riptycene, Phenolic-OH, and Azo-Functionalized Porous Organic Polymers: Efficient and Selective CO_2 Capture. *ACS Appl. Polym. Mater*. **2019**, *1*, 959–968. https://doi.org/10.1021/acsapm.9b00213
[31] Asma, F.; Salah Eddine, H.; Yassmine, C.; Hanane, Z. Phytochemical Screening, Antibacterial and Antioxidant Activities of *Ocimum basilicum L*. Cultivated in Biskra, Algeria. *Chem. Chem. Technol.* **2023**, *17*, 397–406. https://doi.org/10.23939/chcht17.02.397
[32] Brand-Williams, W.; Cuvelier, M. E.; Berset, C. Use of a Free Radical Method to Evaluate Antioxidant Activity. *LWT – Food Sci. Technol*. **1995**, *28*, 25–30 https://doi.org/10.1016/S0023-6438(95)80008-5
[33] Amić, D.; Stepić, V.; Lucić, B.; Marković, Z.; Dimitrić Marković, J. M. PM6 Study of Free Radical Scavenging Mechanisms of Flavonoids: Why Does O–H Bond Dissociation Enthalpy Effectively Represent Free Radical Scavenging Activity? *J. Mol. Model*. **2013**, *19*, 2593–2603. https://doi.org/10.1007/s00894-013-1800-5

[34] Foti, M. C.; Daquino, C.; Geraci, C. Electron-Transfer Reaction of Cinnamic Acids and Their Methyl Esters with the DPPH Radical in Alcoholic Solutions. *J. Org. Chem*. **2004**, *69*, 2309. https://doi.org/10.1021/jo035758q
[35] Mohammed, S. A.; Mousa, H. M.; Alwan, A. H. Determination of Hemolytic Cytotoxicity and Antibacterial Activity of Conocarpus lancifolius Aqueous Leaves Extract. *IOP Conf. Ser.: Mater. Sci. Eng*. **2019**, *571*, 012045. https://doi.org/10.1088/1757-899X/571/1/012045

Received: October 12, 2025 / Revised: December 13, 2025 / Accepted: December 22, 2025

РОЗРОБЛЕННЯ ТА СИНТЕЗ ІМІДАЗОЛОВОГО ЛІГАНДУ І ЙОГО МЕТАЛОКОМПЛЕКСІВ: СПЕКТРОСКОПІЧНА ХАРАКТЕРИСТИКА ТА ОЦІНКА АНТИБАКТЕРІАЛЬНОЇ, АНТИОКСИДАНТНОЇ ТА ГЕМОЛІТИЧНОЇ АКТИВНОСТІ

Анотація. *У цьому дослідженні синтезовано нові комплекси, що містять мультизаміщений арилімідазоловий ліганд, а саме 2-(1H-фенантро[9,10-d]імідазол-2-іл)фенол. Імідазоловий ліганд L синтезовано у результаті реакції конденсації між дикетоном (9,10-фенантрохіноном), ароматичним альдегідом (2-гідроксибензальдегідом) та ацетатом амонію у присутності льодяної оцтової кислоти як розчинника і каталізатора. Далі металокомплекси отримували взаємодією цього ліганду із солями перехідних металів, а саме хлоридами Fe(II), Cu(II), Ni(II) та Co(II), у відповідному розчиннику (етанолі) за контрольованих умов температури та перемішування, щоб забезпечити утворення стабільних комплексів. Структури лігандів та їхніх металокомплексів охарактеризовано за допомогою різних спектроскопічних методів: (UV-Vis), FT-IR, ^{1}H NMR, ^{13}C NMR спектроскопії, мас-спектроскопії, вимірювання магнітної сприйнятливості, молярної електропровідності та елементного аналізу (C, H, N). Встановлено, що синтезовані комплекси мають тетраедричну та октаедричну геометричну будову. Ліганд і його комплекси перспективні для застосування у супрамолекулярних ансамблях, оскільки здатні утворювати бідентатні N-донорні центри для хелатування з іонами металів і формування місткових лігандів. Біологічну активність оцінювали методом дифузії в агарові лунки для визначення антибактеріальної активності ліганду та металокомплексів щодо вибраних штамів грампозитивних і грамнегативних бактерій. Результати показали, що вільний ліганд та його металокомплекси виявляють значно вищу антибактеріальну активність порівняно із референс-препаратом. Антиоксидантний потенціал оцінювали за допомогою аналізу поглинання радикалів DPPH; металокомплекси загалом демонстрували вищий відсоток інгібування радикалів. Гемолітичну активність досліджували на еритроцитах людини для визначення цитосумісності. Отримані результати свідчать про низьку або помірну гемолітичну активність ліганду та металокомплексів, що вказує на прийнятну біосумісність для потенційного біомедичного застосування.*

Ключові слова: *9,10-фенантрохінон, імідазоловий ліганд, комплекси, антибактеріальна активність, антиоксидантний потенціал.*